Desalination and Water Treatment
www.deswater.com
doi: 10.1080/19443994.2013.775671

51 (2013) 7562–7569
December

Taylor & Francis
Taylor & Francis Group

Zeolite Y from rice husk ash encapsulated with Ag-TiO_2: characterization and applications for photocatalytic degradation catalysts

R.M. Mohamed[a,b,*], I.A. Mkhalid[a], M. Abdel Salam[a], M.A. Barakat[b,c]

[a]*Chemistry Department, Faculty of Science, King Abdulaziz University, P.O Box 80203, Jeddah 21589, Saudi Arabia Tel. +966 540715648; Fax: +966 2 6952292; email: imkhalid@kau.edu.sa*
[b]*Advanced Materials Department, Central Metallurgical R&D Institute, CMRDI, P.O. Box 87, Helwan, Cairo, Egypt*
[c]*Department of Environmental Sciences, King Abdulaziz University, Jeddah, Saudi Arabia*

Received 24 December 2012; Accepted 9 February 2013

ABSTRACT

A high level of efficiency in the photocatalytic reactions was achieved by increasing the surface area of the photocatalyst by supporting fine TiO_2 particles on porous materials. Among various supports, zeolites seem to be an attractive candidate. Ti-incorporated Y zeolite was prepared by an ion-exchange method, while Ag was immobilized on the encapsulated titanium via impregnation method. The produced samples were characterized using X-ray diffraction, ultraviolet and visible spectroscopy, photoluminescence emission spectra, scanning electron microscopy, and surface area measurement. Furthermore, the catalytic performances of Ti-Ag/NaY tests were carried out for degradation of cyanide using visible light. The results reveal a good distribution of Ag on the zeolite. Ag doping can eliminate the recombination of electron-hole pairs in the catalyst. These results demonstrate that the optimum weight% of Ag to Ti-NaY is 0.3%; this weight% facilitates high performance by the photocatalyst, degrading 99% of cyanide in a 100 mg/L solution in 60 min.

Keywords: Rice husk ash; Ion-exchanged zeolite; Cyanide

1. Introduction

Zeolites are widely used in a range of applications from simple ion-exchange processes to gas separations [1,2]. Zeolites can also serve as catalysts, often after metals have been introduced into a framework, which brings about some special properties for heterogeneous catalysis [3]. The noncorrosive, environmentally-friendly, economically-viable nature of the zeolite-catalyzed reactions and their inherent capabilities of product selectivity have provided the opportunity for the development of various zeolites-based industrial processes. The metal, ion-exchanged NaY zeolite is one of the most important catalysts, because of its many properties, including activity, thermostability, reusability, easy handling, and easy preparation. Generally, the physicochemical properties of zeolites depend on the number of tetrahedrally coordinated Al atoms in the zeolite framework. Therefore, in order to improve the physicochemical properties of zeolites, isomorphous substitution of

*Corresponding author.

framework Al by various metals, such as Ga, Fe, B, V, Zn, and Ti, has been widely studied [4–6].

TiO_2 is currently considered the most promising catalyst for the photocatalytic degradation of organic compounds, owing to its suitable band gap energy for redox reactions, mechanical and chemical stability, environmental friendliness, low cost, and convenience of preparation [7–10]. Given the current concern regarding environmental issues, it is anticipated that applications for TiO_2 will grow at increasing speed; in particular, urgent improvement of the TiO_2 photocatalytic degradation is needed for large-scale industrial treatment processes, such as wastewater treatment and de-NOx. From the green chemistry viewpoint, the photocatalytic decomposition of organic compounds in wastewater has attracted a great deal of attention [11–22]. The TiO_2 is one of the most effective photocatalysts because it is generally biologically and chemically inert, and is photostable with near-UV band gap energy. The fine TiO_2 powder, or crystals, can be dispersed in the water, in order to be clarified by irradiation; however, they must be removed by filtering after reaction, which is troublesome and costly. Thus, in order to solve this problem, many researchers have examined methods of fixing TiO_2 on other supporting materials, including glass beads [20–22], fiberglass [23–25], silica [26,27], an electrode [28], and zeolite [29,30]. Recently, some researchers have used zeolite as hosts to fix semiconductors, due to its unique, uniform pores and channel size. Since encapsulation of TiO_2 into zeolite was first introduced by Krueger et al. [31] and Liu et al. [32,33], many other encapsulation methods [34–37] have been developed to produce small particle sizes exhibiting quantum size effects or some improved photochemical reactions.

Pursuant to this goal, we describe the preparation and catalytic activity of a new photocatalyst. Degradation of cyanide under visible light in water was synthesized by introducing titania into the pores of zeolite (NaY) through the ion-exchange method, while Ag was immobilized on the encapsulated titanium via the impregnation method. This method is environmentally attractive because the authors convert rice husk ash (RHA) (waste materials) into zeolite materials (applicable materials). The rationale behind adding Ag was to increase the lifetime of e–h recombination and convert the absorbance of Ti-NaY from UV to the visible region.

2. Experimental details

2.1. Materials

Hydrochloric acid (37%) was purchased and then used in the procedure, as it was received (Aldrich). Sodium hydroxide pellets (Sigma–Aldrich, 99.5%) and sodium aluminate (Riedle-de Haen, 54% Al_2O_3, 41% Na_2O) were used. All the reagents were used as received. All aqueous solutions were prepared using doubly distilled water.

2.2. Preparation of zeolite

Initially, any dirt and soil attached to RH can be removed by washing with plenty of tap water and rinsing with distilled water. The metallic impurities in RH can be reduced to negligible levels by refluxing with hydrochloric acid (32%) [38]. The chemical composition of RHA, which was examined by X-ray fluorescence spectroscopy (XRF: Philips, PW1400), is shown in Table 1. We directly extracted the silica by stirring the acid-treated RH (after drying) with sodium hydroxide solution (4 M). During this process, silica was extracted in the form of sodium silicate together with other organic moieties, according to the method patented by Adam and Fua [39]. The sodium silicate obtained was converted to silica by adding suitable amounts of mineral acid. RHA was obtained by pyrolyzing the RH, at temperatures ranging from 500 to 800 °C, for 5–6 h in a muffle furnace (Carbolite), in order to remove the organic contents. The yield of silica in this sample ash was 89%. In 2006, Chandrasekhar et al. [40] studied the effect of acid treatment, calcination temperature, and the rate of heating of RH; they showed that these parameters influenced the surface area, reactivity toward lime, and brightness of the ash. NaY zeolite was synthesized with two different gels (seed gel and feedstock gel); the difference between the two aforementioned gels is that the feedstock gel was prepared and used immediately without an aging step. The seed gel (Al_2O_3:10 SiO_2) was prepared first by adding the Na_2SiO_3 solution into the sodium aluminate (Riedle-deHaen 54% Al_2O_3, 41% Na_2O) solution, stirring until homogenous, and then leaving the solution undisturbed for 24 h at room temperature. The feedstock gel (Al_2O_3: 10 SiO_2) was prepared the same way, but

Table 1
Chemical composition of RHA determined by XRF

Chemical compositions of RHA	wt.%
SiO_2	89.00
Al_2O_3	1.20
Fe_2O_3	1.28
K_2O	1.22
CaO	1.00
C	18.24

was used immediately without aging. The seed gel was then mixed into the feedstock gel, through vigorous stirring, until a homogeneous gel was obtained. The resulting gel remained at ambient temperature for 24 h, and crystallized at 110 ℃ for another 24 h. The final product was filtered, washed, and dried at 100 ℃ in an oven.

2.2. Insertion of TiO_2 nanoparticles into zeolite Y

We employed a conventional, ion-exchange method, using an aqueous solution of 0.03 M potassium titanooxalate. One gram of NaY was added to the potassium titanooxalate solution and stirred for 24 h. After the ion-exchange, the zeolite sample was filtered, washed with doubly distilled water, in order to prevent the physically adsorbed titanium species from aggregating on the external surface of the zeolite, and then dried for 24 h in an oven at 100 ℃. The resulting TiO_2-exchanged zeolite (Ti-NaY) was calcined at 550 ℃ for 5 h, with a heating rate of 5 ℃/min. The wt.% of Ti to zeolite Y was controlled at 5 wt.% for all prepared samples.

2.3. Preparation the Ag/Ti-NaY catalyst

Incipient wetness impregnation was used to introduce different wt.% Ag onto already formed Ti-NaY. Impregnation of Ag onto Ti-NaY was carried out as follows: $AgNO_3$ was dissolved in 100 ml of deionized water and stirred. Then, a predetermined amount of Ti-NaY was stirred for 24 h at room temperature, evaporating by using an oil bath rotary evaporator. The obtained catalyst was dried for 24 h at 100 ℃ and then calcined at 500 ℃ for 5 h. The resulting Ag, containing Ti-NaY, was labeled according to the different Ag ions loading on Ti-NaY, including: 0.1% Ag/Ti-NaY, 0.2% Ag/Ti-NaY, 0.3% Ag/Ti-NaY and 0.4% Ag/Ti-NaY.

2.4. Material characterization

X-ray diffraction (XRD) patterns were recorded using a Bruker axis D8 diffractometer with Cu Kα radiation ($\lambda = 1.540$ Å) over a 2θ collection range of 4–60°. Surface morphology of the catalyst was examined using scanning electron microscopy (SEM) JEOL 5,410 (Japan). Nitrogen adsorption and desorption isotherms were measured at −196 ℃, using a Nova 2000 series Chromatech apparatus. All the samples were degassed at 200 ℃ for 2 h prior to data collection. Band-gab values of the samples were obtained via the UV–Visible diffuse reflectance spectra (UV–Vis-Diffuse reflectance spectra), in air at room temperature, in the wavelength range of 200–800 nm, using a UV/Vis/Near infrared spectrophotometer (V-570, JASCO, Japan). Photoluminescence (Pl) emission spectra were recorded with the fluorescence spectrophotometer, Shimadzu RF-5301.

2.5. Photocatalytic tests

For liquid-phase photocatalytic degradation, the photocatalyst was dissolved in 300 ml of distilled water and 100 ppm of a potassium cyanide (KCN) solution (pH = 10.5, in order to avoid the evolution of hydrogen cyanide gas), which was adjusted by an ammonia solution. These were placed in a horizontal cylinder annular batch reactor, irradiated with a blue fluorescent lamp (150 W, maximum energy at 450 nm), and doubly covered with a UV cut filter. The intensity data of UV light were confirmed to be under the detection limit (0.1 mW/cm^2) of a UV radiometer. The reaction was carried out isothermally, at 25 ℃, and samples of the reaction mixture were taken at different intervals for a total reaction time of one hour. The $CN^-_{(aq)}$ concentration in the samples was estimated by volumetric titration with $AgNO_3$, using potassium iodide to determine the titration endpoint [41]. The removal efficiency of $CN^-_{(aq)}$ was measured by applying the following equation:

$$\%\,\text{Removal efficiency} = (C_0 - C)/C_0 \times 100$$

where C_0 is the initial concentration of uncomplexed $CN^-_{(aq)}$ in solution and C is the concentration of unoxidized $CN^-_{(aq)}$ in solution.

3. Results and discussion

3.1. XRD analysis

Powder XRD is the most suitable analysis to characterize the crystalline structure of the catalyst particles, in order to indicate the effect of Ti and Ag loadings on the structure of zeolite Y. Fig. 1 depicts the XRD patterns pertaining to NaY, Ti-NaY, and Ag/Ti-NaY, showing that the crystallinity of zeolites were found to be unaltered after the ion-exchange process and impregnation method. Actually, the above-prepared Ti-exchanged zeolite sample and Ag/Ti-NaY do not contain an amorphous phase or TiO_2 and Ag_2O phase. This indicates that the structural damage is negligible during the ion-exchange process; it also indicates that the TiO_2 particles

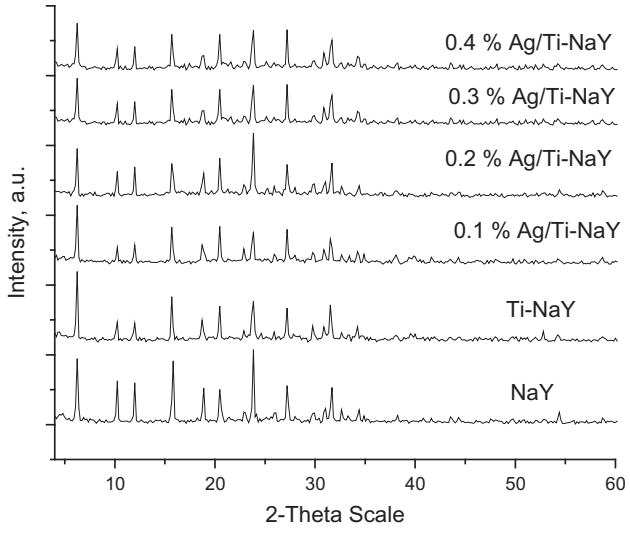

Fig. 1. XRD patterns of NaY, Ti- NaY, and Ag/Ti-NaY samples.

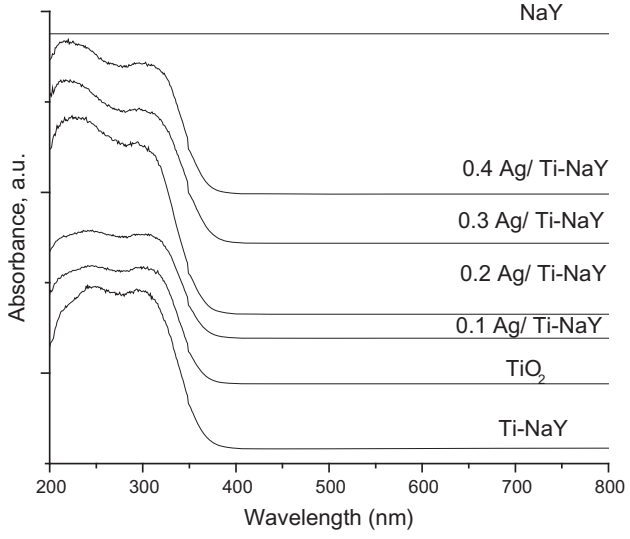

Fig. 2. Diffuse reflectance UV–Vis absorption spectra of NaY, Ti- NaY, and Ag/Ti-NaY samples.

residing in the zeolite cavities or channels were too small to be detected by XRD. There were no peaks for the Ag_2O species, which indicated a good distribution of Ag on the zeolite.

3.2. UV–Vis

The UV–Vis diffuse reflectance spectra of the bulk TiO_2 and titanium-exchanged zeolite catalyst are displayed in Fig. 2. A significant blue shift of the spectrum was observed, when compared with that of bulk titania. This shift can be attributed to two factors.

Table 2
Relationship of nanocomposite composition and band gap energy

Sample	Band gap energy (eV)
NaY	–
Ti-NaY	3.15
TiO_2	3.10
0.1% Ag/Ti-NaY	2.93
0.2% Ag/Ti-NaY	2.75
0.3% Ag/Ti-NaY	2.41
0.4% Ag/Ti-NaY	2.38

First, it can be dependant on the size quantization effect. Due to the presence of extremely small Ti-oxide particles and/or the bands in the wavelength regions (330–370 nm), their intensity increases with an increase of Ti content. This result was in agreement with Easwaramoorthi and Natarajan [42]. The sudden fall in the wavelength indicated the presence of an optical band gap after the ion exchange of Ti species into the zeolite [43]. These observations proved the success of the ion-exchange process, despite the lack of a diffraction peak, attributed to TiO_2 observed in the XRD analysis. On the other side, the loading of Ag ions into the Ti-NaY caused a red shift toward a higher wavelength, from 400 to 520 nm for different loadings of Ag, when compared to Ti-NaY, which had a wavelength of about 390 nm. The direct band gap energies for the bare TiO_2, TiO_2 encapsulated into NaY, and Ag/Ti-NaY were calculated from their reflection spectra, based on a method suggested by Kumar et al. [44], and are shown in Table 2. It is clear that the energy gap decreased with an increase in the Ag ions, up to 0.3 wt.%. Also, at higher concentrations of Ag ions (i.e., 0.4 wt.%), no significant decrease in the energy gap was observed. This observation indicated that there was an optimum value for the doping of the Ag ion; above this optimum loading value the optical gap showed no more direct dependence on the metal ions [45].

3.3. Pl characteristics

Pl emission spectra have been used to study the transfer of the photogenerated electrons and holes, and to understand the separation and recombination of photogenerated charge carries. In order to investigate the photoelectric properties of the prepared samples, the Pl spectra were detected for the different samples exited at 300 nm at room temperature, as shown in Fig. 3. It is clear that the position of emission of Ti-NaY is different from Ag/Ti-NaY samples,

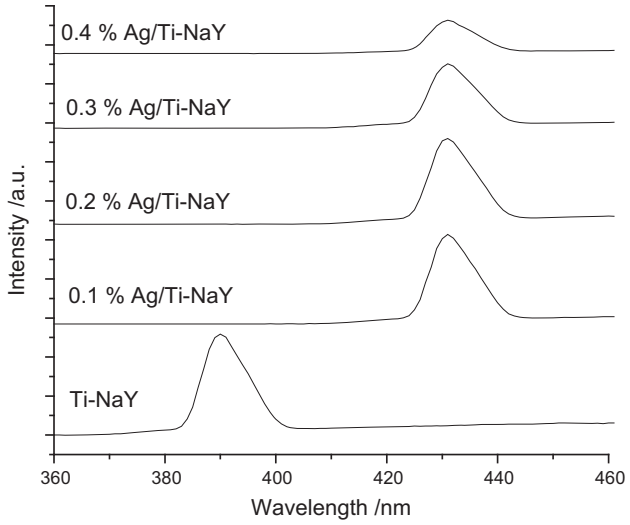

Fig. 3. Pl spectra of Ti-NaY and Ag/Ti-NaY samples.

Table 3
BET surface area of NaY, Ti-NaY, and Ag/Ti-NaY samples

Sample	S_{BET} (m^2/g)	V_p (cm^3/g)
NaY	716.6	0.350
Ti-NaY	704.3	0.345
0.1% Ag/Ti-NaY	700.0	0.340
0.2% Ag/Ti-NaY	695.5	0.328
0.3% Ag/Ti-NaY	687.3	0.305
0.4% Ag/Ti-NaY	685.4	0.299

and that Pl intensity greatly decreased with the increase of the Ag percent. Ag acts as a trapping site, to capture photogenerated electrons from TiO_2 conduction band, separating the photogenerated electron–hole pairs.

3.4. Structural analysis

The BET surface areas of the NaY, Ti-NaY, and Ag/Ti-NaY are tabulated in Table 3. A slight reduction in the S_{BET} value was observed for NaY (from 716.6 to 704.3 m^2/g then reduced to 685.4 m^2/g after ion exchanged with zeolite), and subsequently with 0.4% Ag. This significant reduction in the surface area, after the loading of both titanium oxide and Ag ions, is good evidence of successful loading of TiO_2 and Ag through the ion-exchange and impregnation methods, respectively. In addition, pore mouth blockage, which is the most worrying phenomenon in the production of a supported zeolite catalyst, was not observed in the analysis.

The pore volume of the catalyst was found to slightly decrease from 0.350 cm^3/g for NaY to 0.345 cm^3/g for Ti-NaY. This reduction in pore volume was due to the agglomeration of TiO_2 clusters inside the pores of zeolite after the calcination step. Fig. 4 shows N_2 adsorption–desorption isotherm of 0.3% Ag/Ti-NaY photocatalyst. The results reveal that the type of isotherm is type IV. The micrograph structures of the NaY, Ti-NaY, and 0.3% Ag/Ti-NaY are seen in Fig. 5. The SEM results of the modified zeolites were in agreement with the XRD results, as there was no major change in the structure. The zeolite was able to keep its crystal shape, even after the loading of Ti species and Ag ions, as is shown in Fig. 4, respectively.

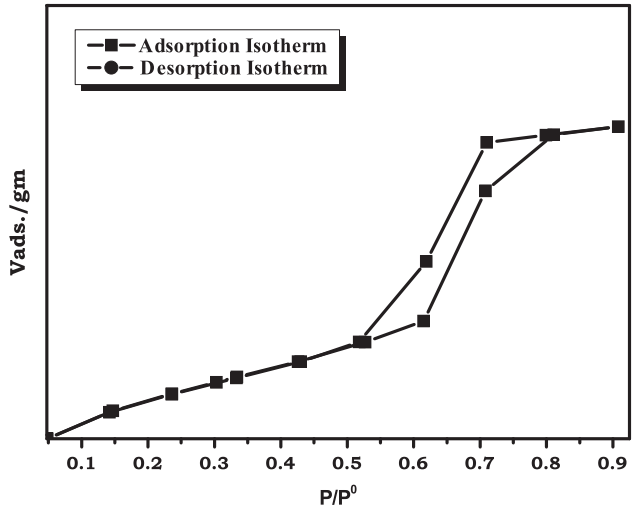

Fig. 4. N_2 adsorption–desorption isotherm of 0.3% Ag/Ti-NaY photocatalyst.

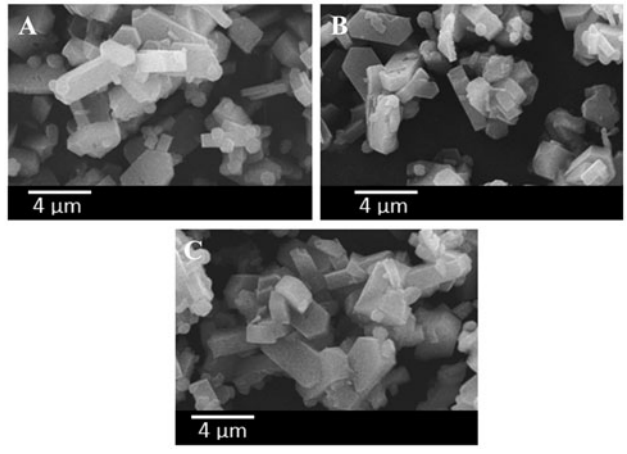

Fig. 5. Surface morphology of (A) NaY, (B) Ti-NaY, and (C) 0.3% Ag/Ti-NaY.

On the other hand, the results of Energy -dispersive X-ray Spectroscopy (EDAX/EDX) analysis, which identify only the surface element of the sample, are shown in Fig. 6. It is clear, in examining (Fig. 6), that there was no specific signal for TiO_2 detected on the surface of the catalyst. As a result, we determined that the titanium oxide was successfully encapsulated inside the supercages of zeolite, through the ion-exchange method. This finding was in agreement with a few earlier studies. For example, Easwaramoorthi and Natarajan [42] did not detect any Ti presented on the external surface of zeolites in the case of TiO_2 encapsulated into zeolite by the ion-exchange method. However, they detected the presence of Ti on the surface of a zeolite loaded with TiO_2 that was prepared using the sol gel method. As such, the preparation method plays an important role in characteristics of the final material. For the case of Ag loaded on Ti-NaY as shown in Fig. 6, a small amount of Ag ions was detected to present on the surface of the catalyst. This result proved the successful loading of Ag ions through the impregnation method.

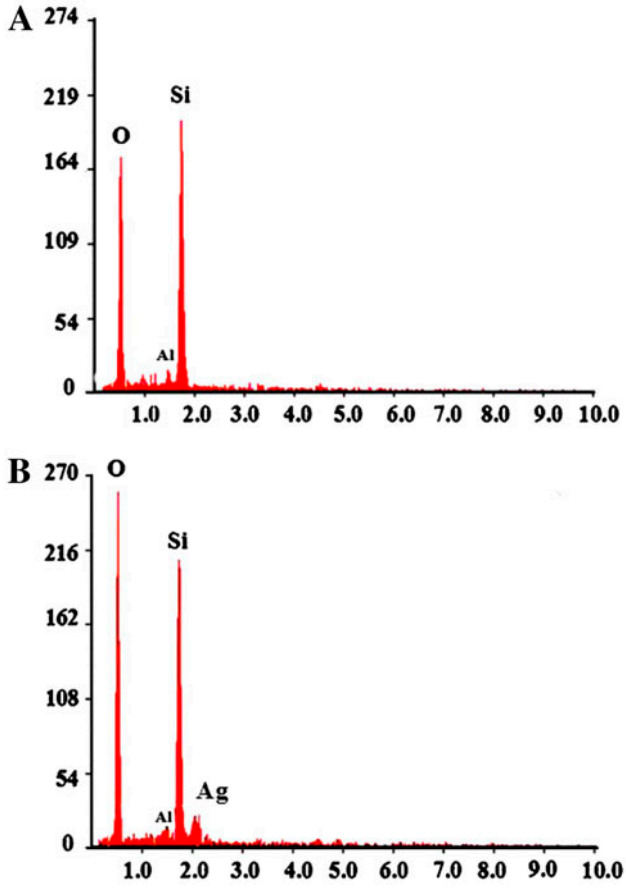

Fig. 6. EDAX analysis results for (A) Ti-NaY and (B) 0.3% Ag/Ti-NaY.

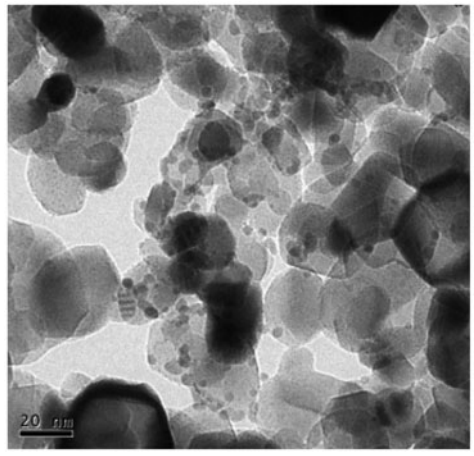

Fig. 7. TEM image for 0.3% Ag/Ti-NaY photocatalyst.

The morphology of 0.3%Ag/Ti-NaY was examined further using TEM imaging, as shown in Fig. 7. The TEM image confirmed the presence of Ag deposits on the surface of Ti-NaY. As is shown in Fig. 7, Ag deposits were well dispersed on many of the Ti-NaY particles; diameters ranged from 3 to 5 nm.

4. Photocatalytic tests

Highly dispersed Ag ions that were included within Ti-exchanged zeolite cavities were prepared using the impregnation method, which acted as the photocatalyst for a series of experiments on cyanide removal efficiency.The estimated data are summarized in Fig. 8. The results indicate that Ti-NaY and TiO_2 have no photocatalytic activity under visible light, due to their absorbance on the UV region. Additionally, an increase of wt.% from 0.1 to 0.3 lead to a high cyanide removal efficiency of 66–99%, respectively. No significant increase in photocatalytic activity was observed and higher concentrations of Ag ions (i.e. 0.3 wt.%) were used.

Photocatalytic activity is known to be dependent on the crystallinity, surface area, and morphology. It may be improved by slowing the recombination of photogenerated electron-hole pairs, extending the excitation wavelength to a lower energy range, and increasing the amount of surface-adsorbed reactant species. In general, the process for photocatalysis begins when supraband gap photons are directly absorbed, which generates electron-hole pairs in the semiconductor particles. This is followed by diffusion of the charge carriers to the surface of the particle, where the interaction with water molecules produces a highly reactive species of peroxide (O_2^-) and hydroxyl radical ($OH^{\bullet}$), which are responsible for the degra-

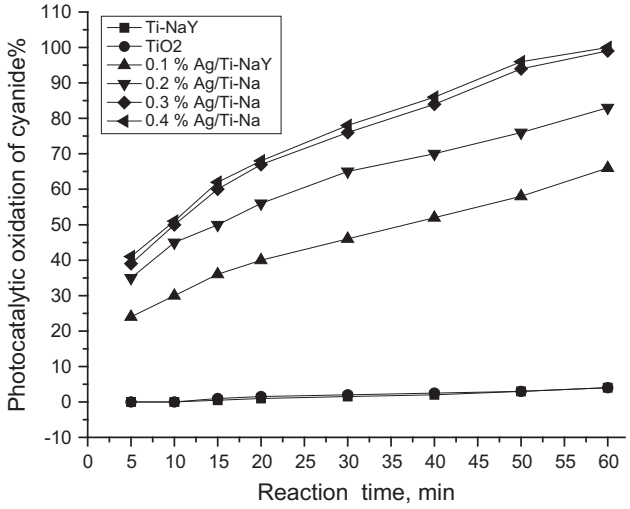

Fig. 8. Photocatalytic degradation of cyanide by TiO_2, Ti-NaY, and Ag/Ti-NaY samples.

dation of adsorbed organic molecules. Step-reactions in the photocatalytic process leading to the degradation of CN^- are presented in the following sequence:

$$TiO_2 + hv \rightarrow e^- + h^+$$

$$e^-(Ag) \rightarrow e^-_{tr}(Ag)$$

$$e^-_{tr} + O_2(ads) \rightarrow O_2^-$$

$$2e^-_{tr} + 2H^+ + O_2 \rightarrow H_2O_2$$

$$H_2O_2 + e^-_{tr} \rightarrow OH^- + OH^{\cdot}$$

$$H^+ + H_2O \rightarrow H^+ + OH^{\cdot}$$

$$2CN^- + 4OH^{\cdot} \rightarrow 2N_2 + 2CO_2 + 2H_2$$

5. Conclusions

The results of the current research underscore the considerable variation in photoactivity of TiO_2 phases when they are encapsulated on zeolites. The results presented above clearly demonstrate that the preparation of nanosized TiO_2 particles inside zeolites can be formed via ion exchange of the zeolite. The same observations were also obtained by incorporating Ag ions on Ti-NaY, using the impregnation method. Overall, a significant photocatalytic rate enhancement is observed in the reaction studied. These findings were also investigated using XRD, UV–Vis, and EDX analyses. The Ag/Ti-NaY photocatalyst is a promising catalyst, due to its high removal efficiency of the pollutant under visible light. These results demonstrate the successful loading of Ag ions through the impregnation method. The maximum degradation efficiency achieved was 99% at 0.3% Ag/Ti-NaY after a 60 min reaction time. The doping of the Ag ion into the Ti-NaY was useful in improving the photocatalytic activity. This may be due to its ability to inhibit the e^-–h^+ recombination, produced from the Ti species, inside the pores of zeolite. The new, heterogeneous photocatalyst Ag/Ti-NaY is a promising catalyst for cyanide degradation under visible light.

Acknowledgment

This project was funded by the Deanship of Scientific Research (DSR), at King Abdulaziz University, Jeddah, under grant number (1432/130/443). The authors thankfully acknowledge DSR technical and financial support.

References

[1] J.P. Chen, L. Yang, W.-J. Ng, L.K. Wang, S.-L. Thong, L.W. Wang, Y.-T. Hung, N.K. Shammas (Eds.), Handbook of Environmental Engineering: Advanced Physicochemical Treatment Processes, vol. 4, Humana, NJ, 2006, p. 261.
[2] H.S. Sherry, S.M. Auerbach, K.A. Carrado, P.K. Dutta (Eds.), Handbook of Zeolite Science and Technology, Marcel Dekker, New York, NY, 2003, p. 1007.
[3] R. Glaeser, J. Weitkamp, M. Baerns (Ed), Basic Principles in Applied Catalysis, Springer, New York, NY, 2004, p. 161.
[4] M. Tamura, W. Chaikittisilp, T. Yokoi, T. Okubo, Incorporation process of Ti species into the framework of MFI type zeolite, Micropor. Mesopor. Mater. 112 (2008) 202–210.
[5] Q.-H. Xia, T. Tatsumi, Crystallization kinetics of nanosized Tiβ zeolites with high oxidation activity by a dry-gel conversion technique, Mater. Chem. Phys. 89 (2005) 89–98.
[6] V.R. Choudhary, S.K. Jana, Benzylation of benzene by benzyl chloride over Fe-, Zn-, Ga- and In-modified ZSM-5 type zeolite catalysts, Appl. Catal. A 224 (2002) 51–62.
[7] L. Ye, J. Liu, L. Tian, T. Peng, L. Zan, The replacement of {1 0 1} by {0 1 0} acets inhibits the photocatalytic activity of anatase TiO_2, Appl. Catal. B 134–135 (2013) 60-65.
[8] D.M. Tobaldi, A. Sever Škapin, R.C. Pullar, M.P. Seabra, J.A. Labrincha, Titanium dioxide modified with transition metals and rare earth elements: Phase composition, optical properties, and photocatalytic activity, Ceram. Int. 39 (2013) 2619-2629.
[9] S. Garcia-Segura, S. Dosta, J.M. Guilemany, E. Brillas, Solar photoelectrocatalytic degradation of Acid Orange 7 azo dye using a highly stable TiO_2 photoanode synthesized by atmospheric plasma spray, Appl. Catal. B 132–133 (2013) 142–150.
[10] S. Chang, C. Lee, A salt-assisted approach for the pore-size-tailoring of the ionic-liquid-templated TiO_2 photocatalysts exhibiting high activity, Appl. Catal. B 132–133 (2013) 219–228.

[11] F.A. Harraz, O.E. Abdel-Salam, A.A. Mostafa, R.M. Mohamed, M. Hanafy, Rapid synthesis of titania-silica nanoparticles photocatalyst by a modified sol-gel method for cyanide degradation and heavy metals removal, J. Alloys Compd. 551 (2013) 1–7.
[12] R.M. Mohamed, E.S. Aazam, Enhancement of photocatalytic activity of ZnO-SiO_2 by nano-sized Ag for visible photocatalytic reduction of Hg(II), Desalin. Water Treat. 50 (2012) 140–146.
[13] R.M. Mohamed, UV-assisted photocatalytic synthesis of TiO_2-reduced graphene oxide with enhanced photocatalytic activity in decomposition of Sarin in gas phase, Desalin. Water Treat. 50 (2012) 147–156.
[14] R.M. Mohamed, M.A. Barakat, Enhancement of Photocatalytic Activity of ZnO/SiO_2 by Nanosized Pt for Photocatalytic Degradation of Phenol in Wastewater, Int. J. Photoenergy (2012) Article ID 103672, 8 pages.
[15] R.M. Mohamed, E.S. Baeissa, I.A. Mkhalid, M.A. Al-Rayyani, Photocatalytic degradation of methylene blue by Fe/ZnO/SiO_2 nanoparticles under visible-light, J. Nanotechnol. (2012) Article ID 329082, 5 pages.
[16] R.M. Mohamed, E.S. Aazam, Synthesis and characterization of CeO_2–SiO_2 nanoparticles by microwave-assisted irradiation method for photocatalytic oxidation of methylene blue dye, Int. J. Photoenergy (2012), Article ID 928760, 9 pages.
[17] R.M. Mohamed, E.S. Baeissa, Synthesis and characterization of ZnO-SnO_2 nanocomposites for photocatalytic oxidation of trichloroethylene under UV irradiation, J. Photocatal. Sci. 3 (2012) 95–105.
[18] R.M. Mohamed, F.A. Harraz, I.A. Mkhalid, Hydrothermal synthesis of size-controllable Yttrium Orthovanadate (YVO_4) nanoparticles and its application in photocatalytic degradation of direct blue dye, J. Alloys Compd. 532 (2012) 55–60.
[19] R.M. Mohamed, E.S. Baeissa, I.A. Mkhalid, M.A. Al-Rayyani, Optimization of preparation conditions of ZnO–SiO_2 xerogel by sol–gel technique for photodegradation of methylene blue dye, Appl. Nanosci. 37 (2013) 57–63.
[20] R.M. Mohamed, D.L. McKinney, W.M. Sigmund, Enhanced nanocatalysts, Mater. Sci. Eng. R 73 (2012) 1–13.
[21] R.M. Mohamed, E.S. Aazam, Photocatalytic oxidation of carbon monoxide over NiO/SnO2 nanocomposites under UV Irradiation, J. Nanotechnol. (2012) Article ID 794874, 9 pages.
[22] R.M. Mohamed, E.S. Aazam, H2 production with low CO selectivity from photocatalytic reforming of glucose on Ni/TiO_2-SiO_2: Synthesis and nanostructure characterization, Chinese J. Catal. 33(2012) 247–253.
[23] Y. Xu, P.C. Menassa, C.H. Langford, Photodecomposition of several chloroaromatics using a commercial prototype reactor, Chemosphere 17 (1988) 1971–1976.
[24] J. Marugán, R. Grieken, A.E. Cassano, O.M. Alfano, Intrinsic kinetic modeling with explicit radiation absorption effects of the photocatalytic oxidation of cyanide with TiO_2 and silica-supported TiO_2 suspensions, Appl. Catal. B 85 (2008) 48–60.
[25] G. Li, S. Park, B.E. Rittmann, Developing an efficient TiO_2-coated biofilm carrier for intimate coupling of photocatalysis and biodegradation, Water Res. 46 (2012) 6489–6496.
[26] R.M. Mohamed, I.A. Mkhalid, Characterization, characterization and catalytic properties of nano-sized Ag metal catalyst on TiO_2-SiO_2 synthesized by photo-assisted deposition (PAD) and impregnation methods, J. Alloys Compd. 501 (2010) 301–306.
[27] R.M. Mohamed, I.A. Mkhalid, The effect of rare earth dopants on the structure, surface texture and photocatalytic properties of TiO_2–SiO_2 prepared by sol–gel method, J. Alloys Compd. 501 (2010) 143–147.
[28] S. Garcia-Segura, S. Dosta, J. M. Guilemany, E. Brillas, Solar photoelectrocatalytic degradation of Acid Orange 7 azo dye using a highly stable TiO_2 photoanode synthesized by atmospheric plasma spray, Appl. Catal. B 132–133 (2013) 142–150.
[29] R.M. Mohamed, M. Mokhtar Mohamed, Copper(II)phthalocyanines immoblized on alumina and encapsulated inside zeolite X and their applications in photocatalytic degradation of cyanide: A comparative study, Appl. Catal. B 340 (2008) 16–24.
[30] I. Othman, R.M. Mohamed, I.A. Ibrahim, M. Mokhtar Mohamed, Synthesis and modification of ZSM-5 with manganese and lanthanum and their effects on decolorization of indigo carmine dye, Appl. Catal. A 229 (2006) 95–102.
[31] J.S. Krueger, C. Lai, Z. Li, J.E. Mayer, T.E. Malloak, Inclusion Phenomenon and Molecular Recognition, Plenum Press, New York, NY, 1990, p. 365.
[32] X. Liu, K.-K. Iu, J.K. Thomas, Preparation, characterization and photoreactivity of titanium(IV) oxide encapsulated in zeolites, J. Chem. Soc. Faraday Trans. 89 (1993) 1861–1865.
[33] X. Liu, K.-K. Iu, J.K. Thomas, Encapsulation of TiO_2 in zeolite Y, Chem. Phys. Lett. 195 (1992) 163–168.
[34] T. Kamegawa, R. Kido, D. Yamahana, H. Yamashita, Design of TiO_2-zeolite composites with enhanced photocatalytic performances under irradiation of UV and visible light, Micropor. Mesopor. Mater. 165 (2013) 142–147.
[35] Y. Kuwahara, J. Aoyama, K. Miyakubo, T. Eguchi, T. Kamegawa, K. Mori, H. Yamashita, TiO_2 photocatalyst for degradation of organic compounds in water and air supported on highly hydrophobic FAU zeolite: Structural, sorptive, and photocatalytic studies, J. Catal. 285 (2012) 223–234.
[36] S. Shironita, M. Goto, T. Kamegawa, Kohsuke Mori, H. Yamashita, Preparation of highly active platinum nanoparticles on ZSM-5 zeolite including cerium and titanium dioxides as photo-assisted deposition sites, Catal. Today 153 (2010) 189–192.
[37] R.M. Mohamed, F.M. Ibrahim, K. Mori, H. Yamashita, Photocatalytic degradation on Ni loaded Ti-containing mesoporous silica prepared by a photo-assisted deposition (PAD) method, Stud. Surf. Sci. Catal. 174 (2008) 1255–1258.
[38] F.-W. Chang, H.-C. Yang, L.S. Roselin, W.-Y. Kuo, Ethanol dehydrogenation over copper catalysts on rice husk ash prepared by ion exchange, Appl. Catal. A 304 (2006) 30–39.
[39] F. Adam, H.K. Fua, Production of silica from biogenic material, Malaysian Patent MY-136715-A (2008).
[40] S. Chandrasekhar, P.N. Pramada, J. Majeed, Effect of calcination temperature and heating rate on the optical properties and reactivity of rice husk ash, J. Mater. Sci. 41 (2006) 7926–7933.
[41] A.I. Vogel, Quantitative Inorganic Analysis, Longmans, London, 1978.
[42] S. Easwaramoorthi, P. Natarajan, Photophysical properties of phenosafranine (PHNS) adsorbed on the TiO_2-incorporated zeolite-Y, Micropor. Mesopor. Mater. 86 (2005) 185–190.
[43] G. Cosa, M.S. Galletero, L. Fernández, F. Márquez, H. García, J.C. Scaiano, Tuning the photocatalytic activity of titanium dioxide by encapsulation inside zeolites exemplified by the cases of thianthrene photooxygenation and horseradish peroxidase photodeactivation, New J. Chem. 26 (2002) 1448–1455.
[44] V. Kumar, S. Kr Sharma, T.P. Sharma, V. Singh, Band gap determination in thick films from reflectance measurements, Opt. Mater. 12 (1999) 115–119.
[45] I. Gúth, S. Lukic, The influence of iron on the optical energy gap in glasses of Sb-S-I type, J. Optoelectron. Adv. Mater. 3 (2001) 903–908.